Communications in Nonlinear Science and Numerical Simulation 125 (2023) 107391

Contents lists available at ScienceDirect

Communications in Nonlinear Science and Numerical Simulation

journal homepage: www.elsevier.com/locate/cnsns

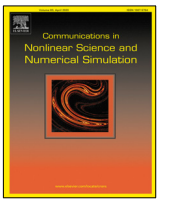

Research paper

Giant boundary layer induced by nonreciprocal coupling in discrete systems

D. Pinto-Ramos [a,*], K. Alfaro-Bittner [b], M.G. Clerc [a], R.G. Rojas [c]

[a] Departamento de Física and Millennium Institute for Research in Optics, Facultad de Ciencias Físicas y Matemáticas, Universidad de Chile, Casilla 487-3, Santiago, Chile
[b] Universidad Rey Juan Carlos, Calle Tulipán s/n, 28933, Móstoles, Madrid, Spain
[c] Instituto de Física, Pontificia Universidad Católica de Valparaíso, Casilla 4059, Valparaíso, Chile

ARTICLE INFO

Article history:
Received 24 September 2022
Received in revised form 25 April 2023
Accepted 20 June 2023
Available online 25 June 2023

Keywords:
Nonreciprocal coupling
Front propagation
Boundary layer phenomena
Nonlinear discrete systems

ABSTRACT

Nonreciprocally coupled systems present rich dynamical behavior such as unidirectional amplification, fronts, localized states, pattern formation, and chaotic dynamics. Fronts are nonlinear waves that may connect an unstable equilibrium with a stable one and can suffer a convective instability when the coupling is nonreciprocal. Namely, a state invades the other one, and due to boundary conditions, the front stops and creates a boundary layer. Unexpectedly, in nonreciprocal coupled systems, we observe arbitrarily large boundary layers in the convective regime when the condition at the fixed edge does not match the equilibrium value. We analytically determine the boundary layer size using map iterations; these results agree with numerical simulations. On the other hand, if one of the boundary conditions matches the unstable equilibrium state, the boundary layer size diverges; however, due to the computer numerical truncation, it is finite in numerical simulations. Our result shows that, in nonreciprocally coupled systems, this mismatch in the boundary condition is relevant in controlling the boundary layer size, which exhibits a logarithm scaling with the mismatch value.

1. Introduction

It is a known matter that extended systems exhibit a boundary layer when two or more phases compete to dominate the system dynamics; they can originate from geometrical or topological aspects [1–3], forces driving different phases [1,3], or the boundary conditions [2,4], to mention a few. One example is nematic liquid crystal layers subjected to strong anchoring and electric fields. The elastic forces try to balance with the electrical ones leaving the mean orientation of molecules with a profile that connects two different states. A common example is the boundary layer of viscous flows passing through an obstacle or inside a pipe. The velocity profile needs to satisfy the no-slip condition and has to connect with the asymptotic flow far from the obstacle [4,5]. Both examples exhibit a thin (compared with the system size) boundary layer, in which the profile of the field has sharp changes near the edges of the respective system. Hence, the boundary layers are produced by imposing "uncomfortable" conditions at the boundaries. Note that boundary layers have different physical properties in comparison to the system bulk [4–6], such as the one exhibited by obstacles immersed in a flow, see Ref. [5]. In general, analytical solutions of boundary layers are not accessible, making therefore numerical simulations a useful tool to characterize them.

* Corresponding author.
E-mail address: david.pinto@ug.uchile.cl (D. Pinto-Ramos).

https://doi.org/10.1016/j.cnsns.2023.107391
1007-5704/

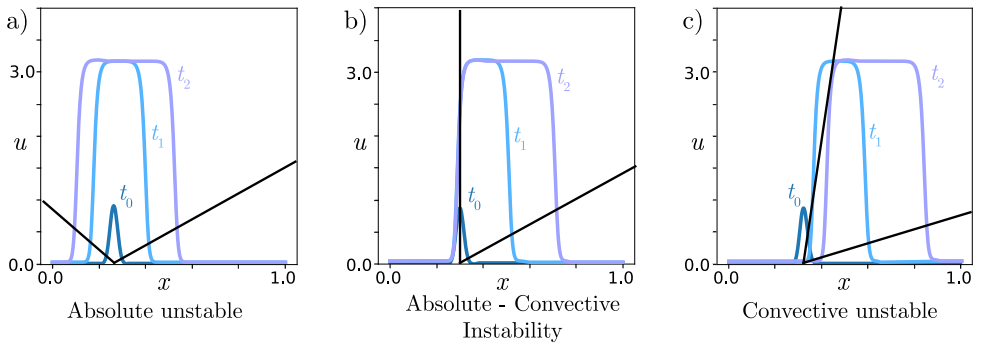

Fig. 1. Absolute-convective threshold. Panel (a) depicts the $u = 0$ as absolutely unstable; that is, perturbations propagate in both directions. Panel (b) shows the system in the absolute-convective instability threshold, where the left flank of the perturbation has exactly zero speed. Panel (c) illustrates the $u = 0$ state as convective unstable, where perturbations grow up and propagate towards the right flank.

A simple 1D scalar model to study the boundary layer is population propagation (when a fixed boundary condition is considered), particularly motivated by the spread of genes and diseases. This type of system is modeled by a simple reaction–diffusion equation known as the Fisher–Kolmogorov–Petrovskii–Piskunov equation (FKPP equation) [7,8]. This model is characterized by including the nonlinear response of the logistic model plus a diffusive transport process. Then, the system is characterized by having two equilibria, one stable ($u = 1$) and the other unstable ($u = 0$), where u accounts for the scalar field. In order to obtain a boundary layer, a fixed (Dirichlet) boundary condition must be considered. Note that the other flank boundary does not affect the above-mentioned boundary layer and, for example, can be considered as zero flow (Neumann). The edge with the fixed condition is settled to the unstable equilibrium value. When the system starts in the unstable state $u = 0$ and is locally disturbed, the emergence of two counterpropagating fronts moving towards the system edges are observed so that the stable state, $u = 1$, invades almost the entire system. These nonlinear waves are known as Fisher–Kolmogorov–Petrovskii–Piskunov fronts (*FKPP fronts*) [7–11]. Due to the fixed boundary condition at the border, a boundary layer is established between the unstable and stable state, and its size is proportional to the square root of the diffusion coefficient. The above scenario changes radically when one considers a drift or advection term in the direction towards the flank with zero flow. When the drift coefficient is small, the boundary layer is slightly modified; however, when this coefficient overcomes a critical value, the system exhibits an absolute–convective instability (triggered by the advection), and therefore the $u = 0$ state invades the system. In the latter case, the system does not present a boundary layer. Fixing a reference frame to the edges, for zero advection, the $u = 0$ state is said to be *absolute unstable*, meaning that perturbations over this state will propagate to the whole system, as seen in Fig. 1(a). On the other hand, for high enough advection, the $u = 0$ state will transit to be *convective unstable* at the absolute-convective instability threshold as seen in Fig. 1(b). Increasing further the advection, the propagation grows in a co-mobile frame, but in the edges reference frame, perturbations decay for infinite time, see Fig. 1(c).

The above-mentioned physical systems are described by continuous equations. However, this description fails to capture some phenomena observed in real systems. Note that real macroscopic systems can be approximated by continuous equations; nevertheless, they are intrinsically discrete. This means they are composed of a large – but finite – number of elements that can interact with each other. Likewise, numerical simulations of continuous descriptions are performed in discrete lattices. Surprisingly, the discrete nature of systems has measurable consequences on the macroscopic world, such as the dislocation dynamics observed in crystals that can only be explained by the Peierls-Nabarro potential [12], the front propagation in discrete systems presenting hopping dynamics [9,10,13], the dispersion of propagating waves [14], or the induction of localized structures [14], to mention a few. In the above examples, the physical principle of reciprocity governs the coupling between the elements, that is, each element that constitutes the system under study is symmetrically coupled to its neighbors [15]. Recently, different experiments have implemented nonreciprocal coupling, generally by breaking the spatial-reflection symmetry. As a consequence of the loss of this symmetry, in extended systems, one expects the perturbations to generate waves that favor specific directions of propagation. More precisely, nonreciprocal couplings are achieved by using rotating fluids [16], temporally modulated coupling elements [17,18], elastic metamaterials [19], or active robotic metamaterials [20].

The study of boundary layers has focused on continuous systems with various boundary conditions. To our knowledge, few systematic studies have been performed on boundary layers in discrete and nonreciprocal nonlinear systems. Moreover, recently it has been shown how nonreciprocal coupling in nonlinear coupled damped oscillators is responsible for convective instabilities, front modulation, and even pattern formation [21]. Our work aims to unveil the boundary layer formation on discrete systems and the nonreciprocal coupling effect on them based on two prototypical models. In the continuous limit, this kind of coupling is responsible for advection and may induce an absolute–convective instability [20,21]. Theoretically, we derive the condition for the convective instability of solutions connecting an unstable with a stable equilibrium in nonreciprocally coupled nonlinear systems. When the fixed boundary condition value mismatches

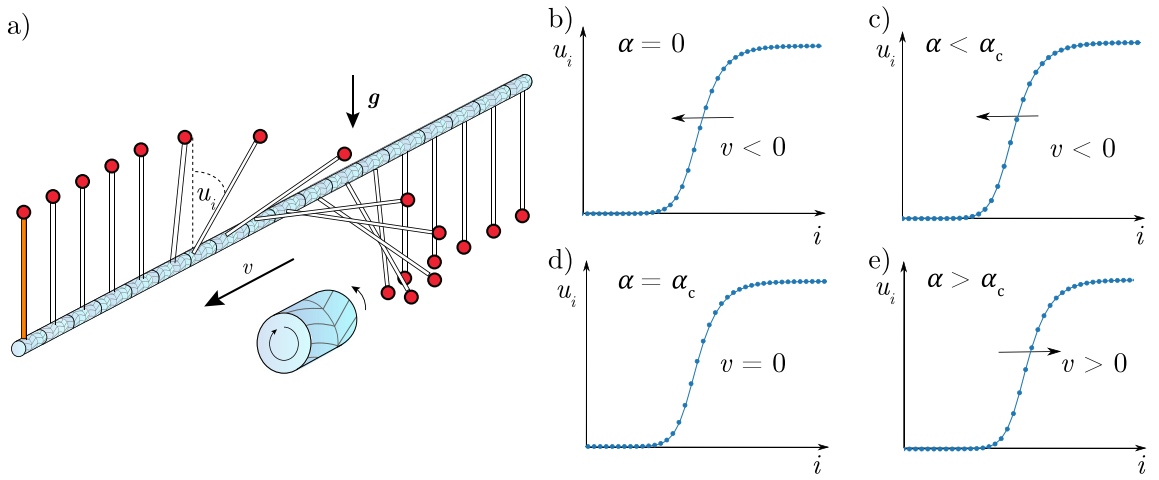

Fig. 2. Nonreciprocal Frenkel-Kontorova system. (a) Schematic representation of a chain of pendula with nonreciprocal coupling. The cylinder illustrates a nonreciprocal torsion spring. u_i accounts for the ith pendulum angle. This variable has its origin in the upside-down position. v stands for the speed of wavefront propagation. (b), (c), (d), and (e) illustrate the angle profile as a function of their index i and the effect of the nonreciprocal elastic coupling α on *FKPP* fronts. α_c accounts for the nonreciprocal critical elastic coupling that gives rise to absolute–convective instability.

with the unstable equilibrium, a boundary layer arises; otherwise, systems exhibit an absolute–convective instability. Unexpectedly, we observe arbitrarily large boundary layers; thus, we call them *giant boundary layers*. We propose a method to predict the boundary layer size based on a recurrence relation describing the equilibrium state that shows excellent agreement with the numerical findings. Our analysis illustrates the importance of the convective instability in *FKPP* fronts in determining the boundary layer size, where an abrupt shift of its size is observed at the instability. This instability creates two regimes, one where the boundary layer does not depend on the mismatch between the boundary condition and the unstable equilibrium value, and the other where a logarithmic law is obtained for the boundary layer size as a function of the boundary condition value.

2. Systems with nonreciprocal coupling

Two prototypical models that exhibit front propagation into an unstable state, *FKPP fronts*, are the Frenkel-Kontorova [12] and the Fisher–Kolmogorov–Petrovskii–Piskunov model [7,8]. The *FKPP* equation was proposed to model the spread of genes mutations and populations (see the textbook [22] and reference therein). The Frenkel-Kontorova model has been derived from several physical situations, including, for example, crystal lattices, torsion chain of pendula (cf. Fig. 2), coupled Josephson junctions, and coupled nonlinear oscillators [12]. In the previous examples, the coupling mechanism usually preserves the space reflection symmetry of the system; namely, they exhibit a reciprocal coupling [15]. Recently, several techniques, methods, and experiments have been developed to break the reciprocity and study the effect of nonreciprocal coupling [16,19,20,23]. Particularly, robotic metamaterials have been employed to explore energy propagation when space reflection symmetry is absent in linear oscillator chains. In these systems, it was shown that perturbations propagate asymmetrically [20], that is, waves are amplified in a preferred direction. Indeed, nonreciprocal coupling allows conducting of the energy in a desired direction. Furthermore, it led to the study of nonreciprocally coupled chains of nonlinear oscillators and front solutions in them [21]. To extend the understanding of nonreciprocal coupling and its effects, we analyze the overdamped discrete extended one-dimensional model given by

$$\dot{u_i} = f(u_i) + (D-\alpha)(u_{i+1} - u_i) - (D+\alpha)(u_i - u_{i-1}), \tag{1}$$

where $u_i(t)$ describes the variable under study for the ith element of the system, for example, the displacement of the ith oscillator with respect to its equilibrium, the population of a given specie in a specified region, or the phase of a given superconductor, to mention a few. α and D account for the nonreciprocal and reciprocal coupling strength, respectively. The chain consists of $(N+1)$ basic elements, which local dynamics is described by the nonlinear function or reaction term $f(u_i)$, and each element interacts with its nearest neighbors. The nonlinear functions that are considered in this work are $f(u_i) = \sin(u_i)$ (Frenkel-Kontorova nonlinearity) and $f(u_i) = u_i(1-u_i)$ (Fisher–Kolmogorov–Petrovskii–Piskunov nonlinearity). Boundary conditions $u_0 = \epsilon$ (Dirichlet) and $u_{N+1} = u_{N-1}$ (zero flow) are imposed. Note that the transformation symmetry $i \leftrightarrow N - i$ is absent as a consequence of boundary conditions. Likewise, the reflection symmetry $i \pm 1 \to i \mp 1$ is absent when $\alpha \neq 0$.

It is worth noting that in Eq. (1), if one defines the coordinate $x = il_0$, where l_0 is the distance between the basic elements, the continuous limit appears as D and α go to infinity at the same time as l_0 vanishes, such that $D_{\text{diff}} \equiv Dl_0^2$ and $\alpha_{\text{adv}} \equiv 2\alpha l_o$ remain finite. With these assumptions, the coupling terms become a diffusive transport and a linear advection.

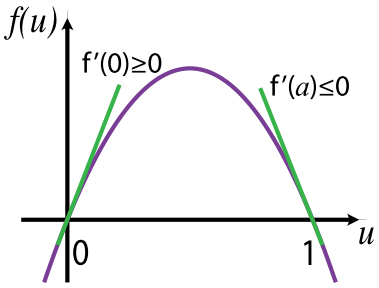

Fig. 3. Schematic representation of the local dynamics. Example of a reaction term $f(u)$ appearing in Eq. (1) as a function of u.

Note that the linear advection can be eliminated using a co-mobile reference frame for infinite systems. Despite the usefulness of the continuous limit to approximate the system solutions [20], we have recently proven that nonreciprocal coupling in discrete systems induces instabilities that are not present in their continuous limit [21].

Without loss of generality, one can choose two reference states such that $f(0) = 0$, $f'(0) > 0$, $f(a) = 0$, and $f'(a) < 0$, where $u_i = 0$ and $u_i = a$ are equilibria ($i = 0, 1, 2, \ldots, N$). Fig. 3 depicts the typical reaction term under consideration. We assume that there exists a solution connecting both equilibria – a *FKPP* front – where $u_i = 0$ and $u_i = a$ are unstable and stable states, respectively. Fronts are particle-type solutions characterized by a position and core. In particular, the position is defined as the coordinate or index with the greatest spatial variation.

2.1. The overdamped Nonreciprocal Frenkel-Kontorova model

When $f(u_i) = \sin u_i$ and $\alpha = 0$ in Eq. (1), the model is known as the overdamped Frenkel-Kontorova model [12]. When inertia is not neglected, the Frenkel-Kontorova model naturally arises in a variety of systems such as crystal lattices, nonlinear oscillators, and Josephson junctions [12]. For large enough dissipation, a first-order equation can be written. Thus, the generalized overdamped Frenkel-Kontorova model with nonreciprocal coupling reads

$$\dot{u}_i = \sin u_i + (D - \alpha)(u_{i+1} - u_i) - (D + \alpha)(u_i - u_{i-1}). \tag{2}$$

A physical example is depicted in Fig. 2(a), which represents a chain of pendula where the upside-down and upright position corresponds to $u_i = 0$ and $u_i = \pi$, respectively. Note that the small cylinder illustrates a nonreciprocal coupling element and, at the border of the chain, the colored pendulum has a fixed position slightly different from zero. Moreover, note that we have swapped the usual equilibria for numerical convenience (commonly one finds in the literature $f(u_i) = -\sin u_i$, which is recovered with a linear transformation). Then, the mismatch boundary condition can read $u_0 = \epsilon$, with ϵ the deviation from the unstable equilibrium value. Fig. 2(b) and 2(c) show the typical *FKPP* front profile propagating to the left (into the unstable state) with speed $v(D, \alpha)$, corresponding to the absolute regime. Panel 2(d) shows a critical situation when the speed of the front is zero, i.e., the system exhibits an absolute convective–instability for a critical value of the nonreciprocal coupling parameter. Finally, panel 2(e) depicts the front in the convective regime, i.e., when the front propagation direction is reversed, spreading the zero equilibrium into the non-null state. Similar models to Eq. (2) can be found in the literature [21,24].

2.2. Nonreciprocal Fisher–Kolmogorov–Petrovskii–Piskunov model

When one considers $f(u_i) = u_i(1 - u_i)$ and $\alpha = 0$, Eq. (1) is known as the Fisher–Kolmogorov–Petrovskii–Piskunov model, originally written to describe combustion processes or the growth of a mutation in a population. It serves as a general model for population growth and saturation, being capable of describing the number of animals, bacteria, vegetation, and humans [22]. The generalization of the *FKPP* model that includes the nonreciprocal coupling is

$$\dot{u}_i = u_i(1 - u_i) + (D - \alpha)(u_{i+1} - u_i) - (D + \alpha)(u_i - u_{i-1}). \tag{3}$$

Similar equations can be found in [25–27], where nonreciprocal terms account for inhomogeneous food supply or external flows driving population movements, such as tides or winds.

3. Mean velocity of *FKPP* fronts

The calculation of the front propagation speed has been addressed in several continuous or discrete physical examples with various techniques [10,11]. The main difference between front propagation in continuous and discrete media is that in the former, the front speed is constant, whereas, in the latter, it is characterized by having hopping dynamics [28]. Here, we employ a similar method to determine the front mean velocity in discrete media following Refs. [10,21]. Considering

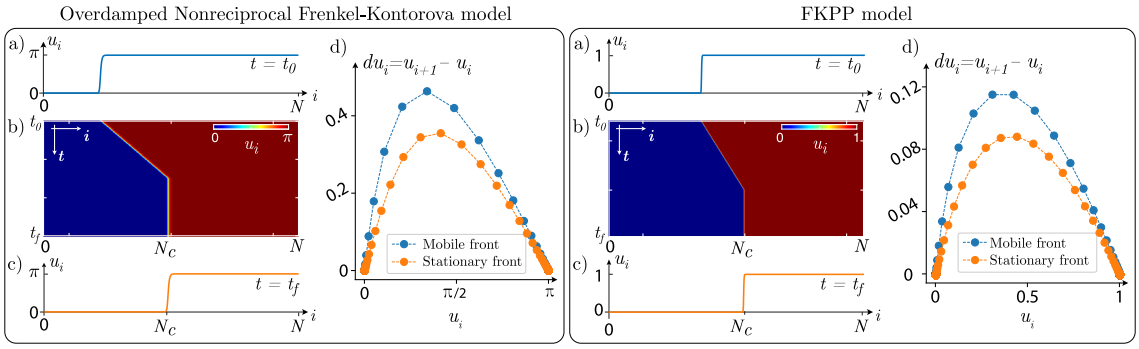

Fig. 4. Giant boundary layers in discrete systems. Examples of giant boundary layers of non-reciprocally coupled discrete systems, parameters $D = 1.5$ and $\alpha = 1.4$ for both the overdamped Nonreciprocal Frenkel-Kontorova model Eq. (2) and the Fisher–Kolmogorov–Petrovskii–Piskunov model Eq. (3). Panels (a) and (c) show the initial and final state of u_i. Panels (b) illustrate the spatiotemporal evolution of the system. (d) Phase portrait representation of the initial and final front profile.

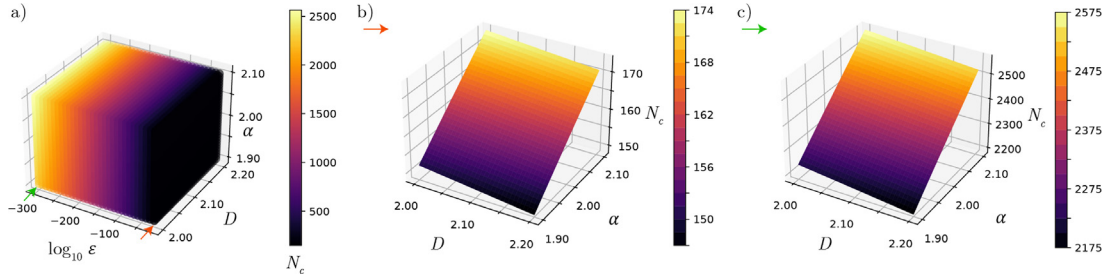

Fig. 5. Giant Boundary layer size characterization. (a) Boundary layer size N_c as a function of the parameters (D, α) and the boundary condition value ϵ for model Eq. (2). (b) and (c) show the dependence of N_c in different planes of constant ϵ value, corresponding to $\log_{10}\epsilon = -20$ and $\log_{10}\epsilon = -300$, respectively.

the ansatz $u_n \sim e^{k(n+\langle v\rangle t)}$ in Eq. (1)—where k and $\langle v\rangle$ correspond to the front steepness and mean velocity—after straightforward calculations, one obtains

$$\langle v(k)\rangle = \frac{f'(0) - 2D}{k} + 2\left(\frac{D\cosh k - \alpha \sinh k}{k}\right), \tag{4}$$

where f' accounts for the derivative of the f function. For bounded perturbations, the front velocity $\langle v(k)\rangle$ tends to its minimum with respect to k, $\langle v\rangle_{min}$ [11]. Considering this $\langle v\rangle_{min}$, one can determine the critical parameter α_c for which the front changes its propagation direction. Namely, it suffers an absolute-convective instability at [21]

$$D = \frac{f'(0)}{4} + \frac{\alpha_c^2}{f'(0)}. \tag{5}$$

Note that for the models considered here, $f'(0) = 1$. Additionally, replacing the continuous limit approximations $D = D_{\text{diff}}/l_0^2$ and $\alpha = \alpha_{\text{adv}}/2l_0$ in the previous formula, one recovers the usual absolute–convective instability threshold in the continuous limit $\alpha_{\text{adv}} = 2\sqrt{D_{\text{diff}} f'(0)}$ [29], corresponding exactly to the speed of *FKPP* fronts in the continuum limit [30].

4. Numerical observations

Numerical simulations of Eqs. (2) and (3) were conducted using a Runge–Kutta of fourth order algorithm, with the aforementioned boundary conditions ($u_0 = \epsilon$ and $u_{N+1} = u_{N-1}$). Simulations are initialized with the initial condition $u_i = 0$ for $i = (2, 3, \ldots, N)$ and $u_1 = 0.1$, corresponding to a small bounded perturbation near the left flank edge of the system. Surprisingly, the *FKPP* fronts propagation is frustrated due to the left boundary condition and the discrete nature of the system. Fig. 4 shows the failure for models Eqs. (2) and (3). We can see that the front propagates with a constant average speed and abruptly stops, frustrating its propagation. Let us denote the position where the front stops as N_c (the equilibrium front position), which corresponds to the boundary layer size. Note that the final profile of the front, i.e., its profile when the propagation stops, is different from the one it has while is propagating, see Figs. 4(d). A similar phenomenon is observed in the phase propagation of parametrically driven systems [31].

For $N > N_c$, the boundary layer size N_c is determined numerically by direct simulation of the dynamical system. Fig. 5(a) shows the boundary layer size in the parameter space (D, α, ϵ). Panels 5(b) and 5(c) show the (D, α) dependence

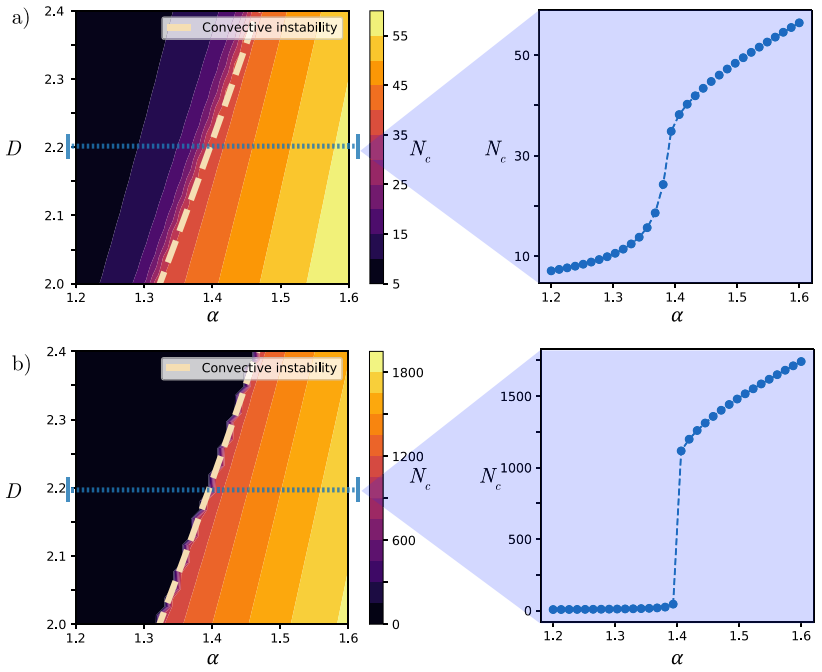

Fig. 6. Convective instability of FKPP fronts and boundary layer size. (a) and (b) exhibit the N_c dependence on parameters close to the convective instability of *FKPP* fronts characterized by $D = 1/4 + \alpha_c^2$. Insets show a horizontal cut where a change in behavior is observed at the instability. For (a), $\log_{10}\epsilon = -10$. For (b), $\log_{10}\epsilon = -320$.

for fixed values of ϵ corresponding to $\log_{10}\epsilon = -20$ and $\log_{10}\epsilon = -300$. Note that the phenomenon cannot be observed if $N < N_c$ because the boundary layer size would be greater than the system size, remaining unnoticeable.

We further study the region near the absolute-convective instability curve given by Eq. (5). One can observe that this bifurcation separates regions of small and large boundary layers depending on the boundary condition value, as seen in Fig. 6. The effect of the absolute-convective instability on boundary layer size is amplified when the boundary condition value ϵ goes to zero approaching the equilibrium value, as seen when comparing the insets of Figs. 6(a) and 6(b).

5. Equilibrium position of front-like solutions

To shed light on the steady states of the model Eq. (1), we use a method similar to the one used in Ref. [32]. This corresponds to solving the recurrence relation or map when one imposes the equilibrium condition $\dot{u}_i = 0$ and the boundary conditions. In our case, $u_0 = \epsilon$ is the initial condition for the map, and its recurrence relation reads

$$0 = f(u_i) + (D - \alpha)(u_{i+1} - u_i) - (D + \alpha)(u_i - u_{i-1}). \tag{6}$$

Note that the above equation corresponds to a bi-dimensional map [33]. In the case of $D = \alpha$, the map simplifies because equation (6) becomes a one-dimensional map. This corresponds to a unidirectional type of coupling, with only backward feedback being applied in the chain. Despite the particular parameter values, this limit illustrates in a simple way the equilibrium front position calculation N_c. In the unidirectional coupling limit, the map recurrence reads

$$\begin{aligned} u_i &= u_{i+1} - \frac{f(u_{i+1})}{2D} \equiv g(u_{i+1}), \\ u_0 &= \epsilon. \end{aligned} \tag{7}$$

The value of N_c can be found iterating the map (7), and seeking the iteration step i^* in which the function $|u_{i^*}| - a/2$ changes its sign, where a corresponds to the non zero equilibrium value (cf. Section 2). As N_c rarely coincides with an element position of the discrete chain; we interpolate linearly $|u_{i^*}| - a/2$ between i^* and $i^* + 1$, then, one can find a continuous value of N_c looking for the zero of the interpolated function.

To iterate map (7) from an initial condition, one generally needs to numerically invert the relation to obtain the map $u_{i+1} = g^{-1}(u_i)$. To illustrate the method, we use the nonreciprocal *FKPP* model Eq. (3). In this case, one can obtain the recurrence relation analytically

$$u_{i+1} = \frac{1 - 2D + \sqrt{(1 - 2D)^2 + 8Du_i}}{2}. \tag{8}$$

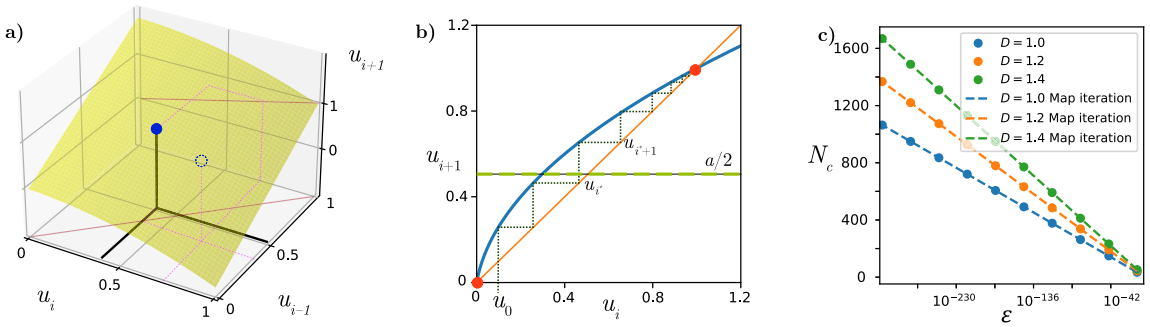

Fig. 7. Map iteration representation. Iterations of the resulting recurrence relation for the stationary solutions of the Nonreciprocal Fisher–Kolmogorov–Petrovski–Piskunov model (3). (a) Bi-dimensional map for $D = 0.6$ and $\alpha = 2$. (b) Unidirectional coupling case for $D = \alpha = 0.6$. u_0 value is the initial condition of the map, which corresponds to the boundary condition of the discrete equation. (c) Boundary layer size as a function of the mismatch ϵ for the unidirectional coupling case $D = \alpha$ for different values of D. Dots are the boundary layer size after equilibrium is reached in the numerical simulation of Eq. (3). Dashed lines are obtained from iterating map (8).

Fig. 7 shows the iteration of map (6) for the *FKPP* model, that is, $f(u_i) = u_i(1 - u_i)$. In particular, Fig. 7(a) shows the case when $\alpha \neq D$, corresponding to the bi-dimensional map where the dots exemplify a starting point (u_k, u_{k-1}) and its resulting value u_{k+1}. Fig. 7(b) illustrates the map iteration when $\alpha = D$. The unidirectional coupling case perfectly illustrates the fact that the heteroclinic orbit requires an infinite number of iterations, as predicted for $\epsilon = 0$ and, therefore, in agreement with the convective regime. For any other value of ϵ, the number of iterations to reach $u_i = 0.5$ ($a/2 = 0.5$ for *FKPP* model Eq. (3)) is finite, and can be determined numerically avoiding the singularity in the number of steps as one approaches fixed points. Finally, one can compare the results obtained for the boundary layer size N_c using direct numerical integration of the motion equations versus the map iteration approach, showing a perfect agreement as illustrated in Fig. 7(c).

6. Analytical approximation for N_c

A naive treatment of the problem suggests that (supported by its local linear dynamics and dimensional analysis) the time in which a perturbation $u = \epsilon$ reaches a $O(1)$ value corresponds to $\tau \sim -\log(\epsilon)$. This, together with a characteristic speed $v(D, \alpha)$ gives a characteristic length $L_c \sim -v(D, \alpha)\log(\epsilon)$. Indeed, for $\alpha > \alpha_c$ one can fit the boundary layer size obtained by direct numerical simulations with the formula

$$N_c(D, \alpha, \epsilon) = c(D, \alpha) - K(D, \alpha)\log(\epsilon). \tag{9}$$

The previous Eq. (9) is found by solving the linear dynamics of the map Eq. (6). To achieve this, one can define $p_i = u_i - u_{i-1}$ and solve equation (6) for u_{i+1}. Remind that most steps of the iteration occur around the fixed point $u = 0$ and, for this reason, we linearize the dynamics around this point, obtaining

$$p_i = u_i - u_{i-1}, \tag{10}$$

$$u_{i+1} = \frac{-f'(0)u_i + (D + \alpha)p_i}{D - \alpha} + u_i. \tag{11}$$

Replacing $p_i = Ab^i$, $u_i = Aqb^i$, and imposing $u_0 = \epsilon$, one finds

$$u_i = \epsilon b^i \equiv \begin{cases} \epsilon\left(\frac{D-1/2}{D-\alpha} - \sqrt{\left(\frac{D-1/2}{D-\alpha}\right)^2 - \frac{D+\alpha}{D-\alpha}}\right)^i & \text{if } \alpha_c < \alpha < D, \\ \epsilon\left(\frac{D-1/2}{D-\alpha} + \sqrt{\left(\frac{D-1/2}{D-\alpha}\right)^2 - \frac{D+\alpha}{D-\alpha}}\right)^i & \text{if } \alpha > D. \end{cases} \tag{12}$$

Then, replacing $i = N_c$ and $u_{N_c} = 1$ in Eq. (12) and solving for N_c (taking into account both signs of the different intervals), one obtains

$$N_c = -\frac{\log\epsilon}{\log b} \equiv -K(D, \alpha)\log\epsilon. \tag{13}$$

The previous relation allows obtaining the main features of N_c, that is, the logarithmic relation with ϵ and the constant of proportionality $K(D, \alpha)$. From here, one can deduce that the constant $c(D, \alpha)$ of Eq. (9) accounts for corrections to the linearized map approximation and the election of u_{N_c}. One can see from Fig. 8 that for $\alpha > \alpha_c$ the value of $c(D, \alpha)$ is a small constant. A perfect agreement between the predicted and numerically obtained values for $K(D, \alpha)$ is also seen.

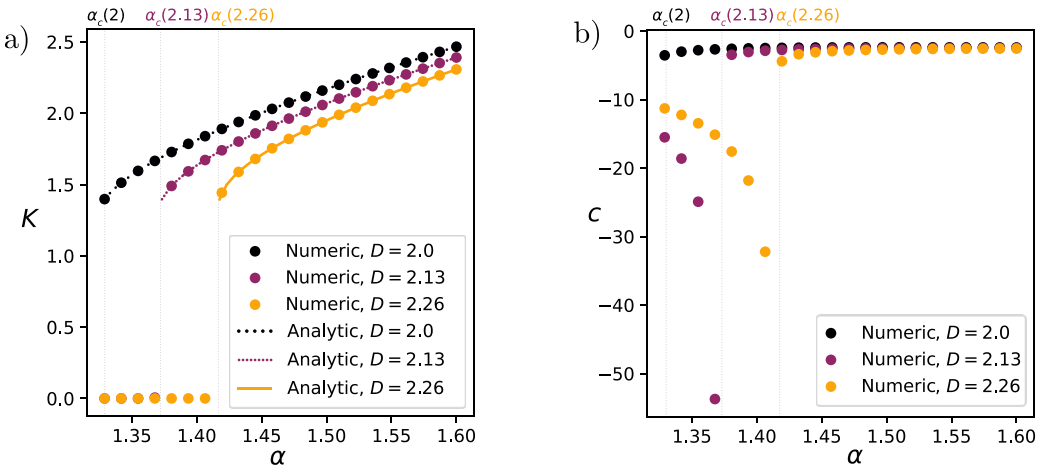

Fig. 8. Giant boundary layer analytic characterization. Values of the fitting constants K and c for the boundary layer size N_c from formula (9). Panels (a) and (b) show K and c as a function of α, respectively. Dots correspond to the numerically obtained values. Dashed lines are the analytical prediction of Eq. (13). The vertical gray lines highlight the value of $\alpha_c(D)$.

7. Contrast with boundary layers in reciprocally coupled systems

The theory developed in the previous sections predicts the boundary layer size of nonreciprocally coupled nonlinear systems for $\alpha > \alpha_c = \sqrt{f'(0)D - f'^2(0)/4}$. Moreover, it is depicted how these boundary layers diverge in size in the limit as $\epsilon \to 0$, a phenomenon not observed in systems with reciprocal coupling. These systems exhibit boundary layers of finite size independently of the mismatch value ϵ. For $\epsilon \ll 1$, the effect of the mismatch is negligible, and the boundary layer size is mainly determined by the reciprocal coupling coefficient D. As mentioned earlier, in the continuum limit, the dependence of the boundary layer size on D_{diff} is a square root function, that is, $L_c \sim \sqrt{D_{\text{diff}}}$. Then, considering that $L_c = N_c l_0$ and $D_{\text{diff}} = D l_0^2$, it is straightforward to obtain that $N_c^{\text{reciprocal}} \sim \sqrt{D}$. To deduce the previous relationship analytically, we consider the continuum limit of Eq. (2) in the steady-state regime

$$0 = \sin u + D_{\text{diff}} \partial_{xx} u, \tag{14}$$

which is a Newton-type equation for a fictitious particle of equivalent mass D_{diff}, and it has a closed-form solution $u(x)$ even if we change the force-like term, $\sin u$, by another well-behaved function. Imposing the boundary condition $u(0) = \epsilon$ and, after straightforward calculations, the solution to Eq. (14) is

$$\Lambda(u) - \Lambda(\epsilon) = \sqrt{\frac{2}{D_{\text{diff}}}} x, \tag{15}$$

where $\Lambda(u) = \sqrt{2}\text{arctanh}\,[\sin(u/2)]$. Defining the position of the boundary layer following the previous section, i.e., $u(L_c) = 1$ and replacing it in Eq. (15), one immediately obtains $L_c = \sqrt{D_{\text{diff}}}[\Lambda(1) - \Lambda(\epsilon)]/\sqrt{2}$. Note that this expression describes fairly well the boundary layer size N_c, despite it was calculated in the continuum limit. Hence, the ratio between the size of the boundary layers when $\alpha > \alpha_c$ and $\alpha = 0$ is

$$S \equiv \frac{N_c(\alpha, D, \epsilon)}{N_c^{\text{reciprocal}}(D, \epsilon)} = \sqrt{2} \frac{K(\alpha, D) \log \epsilon^{-1}}{\sqrt{D}[\Lambda(1) - \Lambda(\epsilon)]}. \tag{16}$$

Note that $\Lambda(1)$ is a constant of order one that changes for each model (different reaction functions f). It is easy to check that as $\epsilon \to 0$, then $S \to \infty$, i.e., there is a giant boundary layer. Additionally, S only grows with α because $K(\alpha, D)$ monotonically increases as function of it, see Fig. 8(a). Fig. 9 illustrates the dependence of $N_c^{\text{reciprocal}}(D, \epsilon)$ obtained by direct numerical simulations of Eq. (2). In particular, panel (a) shows the dependence $N_c^{\text{reciprocal}} \sim \sqrt{D}$ and panel (b) exhibits that the dependence on ϵ is negligible. Additionally, panels (c), (d), and (e) show boundary layers, with $\alpha = 0$, $\alpha < \alpha_c$, and $\alpha > \alpha_c$, respectively, in a chain of coupled pendula obtained numerically from Eq. (2). From this chart, one can see that for $\alpha < \alpha_c$, the boundary layer is composed of a few pendulums, contrasted with the case $\alpha > \alpha_c$ in which a counter-intuitively large number of pendulums form a giant boundary layer.

8. Discussion and perspectives

The results obtained in this work describe a phenomenon that is unavoidable numerically and experimentally. The observation of giant boundary layers arises when a system has the following three ingredients: individual (local) nonlinear

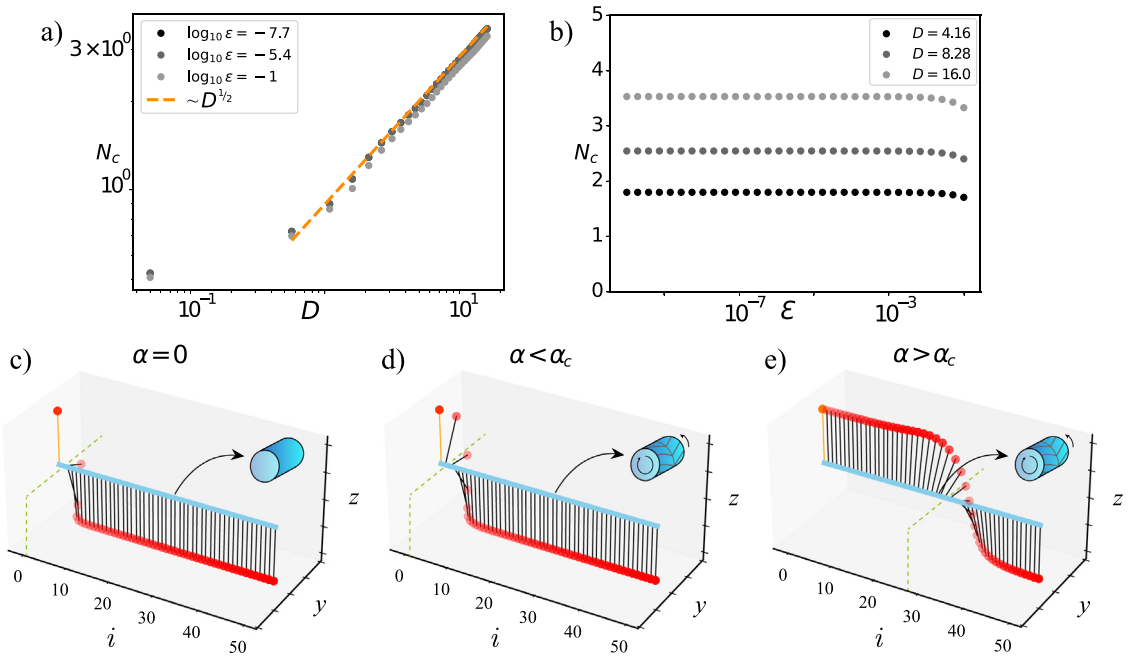

Fig. 9. Characterization of boundary layers in the reciprocal case and visual comparison with giant boundary layers. (a) and (b) illustrate the dependence of the boundary layer size in the reciprocal case on the parameters, $N_c(\alpha = 0, D, \epsilon) \equiv N_c^{\text{reciprocal}}(D, \epsilon)$. (c), (d), and (e) show a visual representation of the boundary layers in a chain of pendulums with data obtained from direct numerical integration of Eq. (2) with $D = 1$, $\epsilon = 10^{-3}$. α values are $\alpha = 0$, $\alpha = 0.5$, and $\alpha = 2$, respectively.

dynamics, nonreciprocal coupling, and boundary conditions. In particular, nonlinear dynamics and nonreciprocal coupling allow for front propagation and the absolute-convective instability. The latter generates counter-intuitive dynamics when $\alpha > \alpha_c$, allowing the propagation of upside-down pendulums over their intuitively rest state due to gravity. Moreover, if one considers particular boundary conditions, the giant boundary layer naturally arises.

Boundary conditions may be hard to handle in real-life situations. Furthermore, experiments are generally subjected to fluctuating drivers that may be stochastic or deterministic. These fluctuations can also be responsible for the formation of giant boundary layers even if a perfect match at the boundary is considered ($\epsilon = 0$). In this case, the boundary layer size is dynamic, i.e., it fluctuates around a mean value. The characterization of giant boundary layers subjected to fluctuations is a work in progress. Boundary layers are affected by the fluctuations, and also other downstream states generated by the nonreciprocal coupling, such as patterns [21].

Another aspect to have in mind is that, similar to what happens in experiments, boundary conditions can be challenging to handle in numerical simulations. Both experiments and simulations have finite accuracy in the relevant variables of the problem under study. Throughout this work, we highlight the numerical difficulties that can arise when handling arbitrarily small numbers (due to the finite representation of real numbers in computers). Moreover, the limit $\epsilon \to 0$ is not accessible, and its application to numerical simulation leads to wrong results (a finite-size giant boundary layer), where only the analytical theory enlightens the correct solution (an infinite-size boundary layer, or equivalently, the observation of the convective instability).

Finally, the implications that giant boundary layers could have in real systems are variable and difficult to visualize. The giant boundary layer composes a region in which the equilibrium states of the nonlinear systems are virtually swapped. The true equilibrium of the system is reached for the individual elements u_i only for $i > N_c$. For example, in the chain of pendulums, inside the giant boundary layer, there is stored potential energy that would release once the nonreciprocity is turned off; in the case of arrays of coupled Josephson junctions, the giant boundary layer would produce a steady current peaking at the boundary layer position. Finally, in the propagation of populations, the giant boundary layer connects large regions of negligible population with regions at full capacity. If the population modeled is a disease, a large portion of healthy individuals could be held inside the giant boundary layer thanks to nonreciprocity. Further development of nonreciprocal elements will unveil the impact of the naturally arising giant boundary layers.

9. Conclusions

Based on a theoretical and numerical study, we predict how “imperfections" in the value of boundary conditions induce the frustration of absolute-convective instability. This establishes a boundary layer whose size is determined with the map

iteration of the resulting equation for the equilibrium. These boundary layers are observed to use almost all of the space, even for small imperfections; thus, we call them giant boundary layers. The method proposed allows us to determine the giant boundary layer size or the mismatch in the boundary condition. Our findings show that this mismatch in the boundary condition for nonreciprocally coupled systems is relevant in controlling the boundary layer size. Moreover, the results are expected to hold for a great variety of discrete systems exhibiting *FKPP* fronts with broken spatial reflection symmetry.

We highlight that the difficulty of using computers to perform a numerical calculation is the finite resolution. The maps describing the equilibria of the systems cannot reach all the values in the real axis, making truncation errors. In other words, even if one initializes the system without mismatch at the boundary, in a finite number of steps, a boundary layer will appear in numerical simulations.

CRediT authorship contribution statement

D. Pinto-Ramos: Methodology, Formal analysis, Investigation, Writing – original draft, Writing – review & editing. **K. Alfaro-Bittner:** Conceptualization, Validation, Visualization, Writing – original draft, Writing – review & editing. **M.G. Clerc:** Conceptualization, Supervision, Writing – original draft, Writing – review & editing. **R.G. Rojas:** Supervision, Writing – original draft, Writing – review & editing.

Declaration of competing interest

The authors declare that they have no known competing financial interests or personal relationships that could have appeared to influence the work reported in this paper.

Data availability

Data will be made available on request.

Acknowledgments

D.P.-R. acknowledges the financial support of ANID National Ph.D. scholarship 2020-21201484. M.G.C. acknowledges the financial support of ANID-Millennium Science Initiative Program-ICN17_012 (MIRO) and FONDECYT project 1210353. R.G.R acknowledges DI INVESTIGACIÓN INNOVADORA INTERDISCIPLINARIA PUCV 2021 N° 039.409/2021. Nanoiónica: Un enfoque interdisciplinario. K.A.-B. thanks to URJC Grants n° 2023/00004/001M2978 and 2023/00005/016M3033.

References

[1] Kamien RD, Selinger JV. Order and frustration in chiral liquid crystals. J Phys: Condens Matter 2001;13(3):R1–22.
[2] Marić V, Giampaolo SM, Kuić D, Franchini F. The frustration of being odd: How boundary conditions can destroy local order. New J Phys 2020;22(8):083024.
[3] Goodby JW, Slaney AJ, Booth CJ, Nishiyama I, Vuijk JD, Styring P, et al. Chirality and frustration in ordered fluids. Mol Crystals Liquid Crystals Sci Technol A. Mol Crystals Liquid Crystals 1994;243(1):231–98.
[4] Schlichting H, Gersten K. Boundary-layer theory. Springer; 2016.
[5] Prandtl L. Über Flussigkeitsbewegung bei sehr kleiner Reibung. In: Verhandl. III. Heidelberg, Teubner, Leipzig: Internat. Math.-Kong.; 1904, p. 484–91, 1904.
[6] Garratt JR. Review: The atmospheric boundary layer. Earth-Sci Rev 1994;37(1):89–134.
[7] Fisher RA. The wave of advance of advantageous genes. Ann Eugen 1937;7(4):355–69.
[8] Kolmogorov A, Petrovskii I, Piskunov N. A study of the equation of diffusion with increase in the quantity of matter, and its application to a biological problem. Byul Moskovskogo Gos Univ 1937;1:1–25.
[9] Alfaro-Bittner K, Clerc MG, García-Ñustes MA, Rojas RG. π-Kink propagation in the damped Frenkel-Kontorova model. Europhys Lett 2017;119(4):40003.
[10] Alfaro-Bittner K, Clerc MG, Rojas RG, García-Ñustes MA. Traveling wave into an unstable state in dissipative oscillator chains. Nonlinear Dynam 2019;98(2):1391–402.
[11] Van Saarloos W. Front propagation into unstable states. Phys Rep 2003;386(2–6):29–22.
[12] Braun OM, Kivshar YS. The Frenkel-Kontorova model: concepts, methods, and applications. Springer Science & Business Media; 2013.
[13] Jara-Schulz G, Ferré MA, Falcón C, Clerc MG. Noise-induced kink propagation in shallow granular layers. Chaos Solitons Fractals 2020;134:109677.
[14] Remoissenet M. Waves called solitons: concepts and experiments. Springer Science & Business Media; 2013.
[15] Maxwell JC. On the calculation of the equilibrium and stiffness of frames. Phil Mag Ser 1864;27(182):294–9.
[16] Nassar H, Yousefzadeh B, Fleury R, Ruzzene M, Alù A, Daraio C, Norris AN, Huang G, Haberman MR. Nonreciprocity in acoustic and elastic materials. Nat Rev Mater 2020;5:667–85.
[17] Williamson IA, Minkov M, Dutt A, Wang J, Song AY, Fan S. Integrated nonreciprocal photonic devices with dynamic modulation. Proc IEEE 2020;108(10):1759–84.
[18] Chen Z, Peng Y, Li H, Liu J, Ding Y, Liang B, Zhu X-F, Lu Y, Cheng J, Alù A. Efficient nonreciprocal mode transitions in spatiotemporally modulated acoustic metamaterials. Sci Adv 2021;7(45):eabj1198.
[19] Coulais C, Sounas D, Alù A. Static non-reciprocity in mechanical metamaterials. Nature 2017;542(7642):461–4.
[20] Brandenbourger M, Locsin X, Lerner E, Coulais C. Non-reciprocal robotic metamaterials. Nature Commun 2019;10(1):1–8.
[21] Pinto-Ramos D, Alfaro-Bittner K, Clerc MG, Rojas RG. Nonreciprocal coupling induced self-assembled localized structures. Phys Rev Lett 2021;126:194102.

[22] Murray JD. Mathematical biology: I. An introduction. 3rd ed.. New York, NY: Springer; 2002.
[23] Sounas DL, Caloz C, Alù A. Giant non-reciprocity at the subwavelength scale using angular momentum-biased metamaterials. Nature Commun 2013;4(1):1–7.
[24] Trias E, Mazo JJ, Falo F, Orlando TP. Depinning of kinks in a Josephson-junction ratchet array. Phys Rev E 2000;61(3):2257.
[25] Nelson DR, Shnerb NM. Life and death near a windy oasis. J Math Biol 2000;41(1):1–23.
[26] Cantrell RS, Cosner C, Lou Y. Movement toward better environments and the evolution of rapid diffusion. Math Biosci 2006;204(2):199–214.
[27] Cosner C. Reaction-diffusion-advection models for the effects and evolution of dispersal. Discrete Contin Dynam Syst 2014;34(5):1701.
[28] Clerc MG, Elías RG, Rojas RG. Continuous description of lattice discreteness effects in front propagation. Phil Trans R Soc A 2011;369(1935):412–24.
[29] Chomaz JM. Absolute and convective instabilities in nonlinear systems. Phys Rev Lett 1992;69(13):1931.
[30] Mollison D. Spatial contact models for ecological and epidemic spread. J R Stat Soc Ser B Stat Methodol 1977;39(3):283–313.
[31] Clerc MG, Coulibaly S, Garcia-Ñustes MA, Zárate Y. Dissipative localized states with shieldlike phase structure. Phys Rev Lett 2011;107:254102.
[32] Aubry S, Le Daeron PY. The discrete Frenkel-Kontorova model and its extensions: I. Exact results for the ground-states. Physica D 1983;8(3):381–422.
[33] Ott E. Chaos in dynamical systems. Cambridge University Press; 2002.